Computers and Chemical Engineering 80 (2015) 211–222

Contents lists available at ScienceDirect

Computers and Chemical Engineering

journal homepage: www.elsevier.com/locate/compchemeng

Construction of analytical solutions and numerical methods comparison of the ideal continuous settling model

Ben Li, Michael K. Stenstrom *

Department of Civil and Environmental Engineering, University of California Los Angeles, Los Angeles, CA 90095, USA

ARTICLE INFO

Article history:
Received 18 August 2014
Received in revised form 8 April 2015
Accepted 30 May 2015
Available online 6 June 2015

Keywords:
Continuous sedimentation
Method of characteristics
Hyperbolic partial differential equation
Numerical methods

ABSTRACT

Continuous sediment has a wide application in chemical engineering process, such as wastewater treatment, water reuse, mineral waste manage and processing. This paper provides analytical solutions of the ideal continuous settling model by using the method of characteristics. The analytical solutions are compared with experiment data to show that the solutions accurately predict the sediment height and concentration as a function of time and loading conditions. Additionally, three alternative methods, using finite differences are compared to the analytical solutions, and their accuracy and efficiency are evaluated. It is shown that all three methods are reliable for solving sedimentation problems but have varying efficiency. Method YRD is the most accurate but also has the greatest computation and implementation cost. Method SG is the least accurate but is the easiest to implement with lowest computation cost. Method G is a compromise between the two methods, providing acceptable accuracy and low computation cost.

1. Introduction

Continuous sedimentation, a gravity driven solid-liquid separation process, has various applications in industrial areas including the wastewater treatment, water reuse, mineral waste manage and processing. However, in current engineering application, the design and operation of the continuous settling tanks still remain as a difficult task, and generally, empirical and conservative strategies are applied, which may cause both capital and land waste, as well as the unanticipated performance flocculation of the settling tank itself (Northcott et al., 2005; Li and Stenstrom, 2014a, 2014c). For the purposes of understanding the continuous settling behavior and optimizing settling tank performance, mathematical models are encouraged to being used, and in most commercial simulators, the ideal one-dimensional (1-D) continuous settling model (without compression effect) is equipped due to its relative well understanding and less computation burden, especially if long term simulation is needed (Bürger et al., 2011).

Given the complexity of real system conditions (*e.g.*, viscosity, dispersion, turbulence, rake effect, various settling behaviors), the concept of the ideal thickener was introduced by Shannon et al. (1963) to simplify the modeling task. In an ideal 1-D condition, the secondary settling tank (SST) possesses a constant cross-section with uniform solids concentration in each horizontal layer, and the complex hydrodynamics are simplified as the upward effluent flow to the top and downward underflow to the bottom, as shown in Fig. 1. The distribution of solids are determined by both gravity settling and the bulk hydraulic transport, and the mass conservation law holding in each layer can be expressed as the partial differential equation, Eq. (1) (Diehl, 1997; Diehl and Jeppsson, 1998):

$$\frac{\partial \phi}{\partial t}+\frac{\partial F(\phi)}{\partial x}=s\delta(x)$$
$$F(\phi)=\begin{cases} -v_e\phi_e=g_e & x<-H \\ f_{bk}(\phi)-v_e\phi=g(\phi) & -H<x<0 \\ f_{bk}(\phi)+v_u\phi=f(\phi) & 0<x<D \\ v_u\phi_u=f_u & x>D \end{cases} \tag{1}$$

where F is the flux function, $\delta(z)$ is the Dirac impulse, $\phi(x,t)$ denotes the solid concentration, x is the depth from the feed inlet, t is the time, $s=v_f\phi_f$, denotes the feed solids flux (ϕ_f is the feed solid concentration and v_f is the feed flow velocity), f_{bk} is the Kynch batch flux function and the solid mass fluxes leaving at the effluent weir and bottom are $g_e=v_e\phi_e$ (v_e is the effluent flow velocity and ϕ_e is

* Corresponding author. Tel.: +1 310 825 1408; fax: +1 310 206 2222.
E-mail addresses: liben1988@ucla.edu (B. Li), stenstro@seas.ucla.edu (M.K. Stenstrom).

http://dx.doi.org/10.1016/j.compchemeng.2015.05.025
0098-1354/

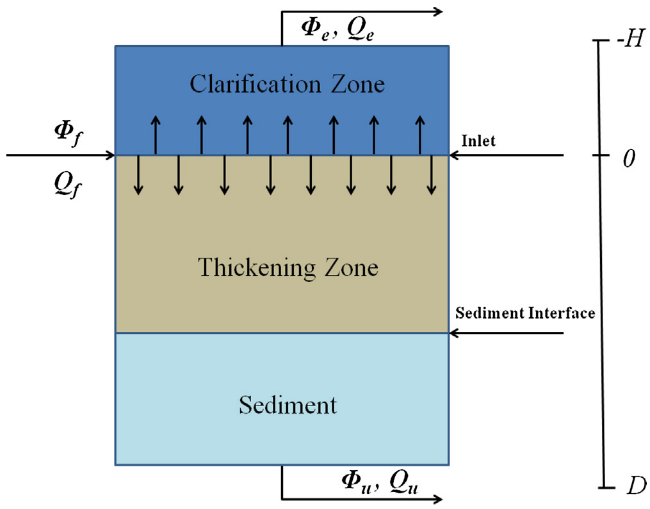

Fig. 1. Schematic overview of ideal continuous settling tank with constant cross-section area

the effluent solids concentration) and $f_u = v_u\phi_u$ (v_u is the underflow velocity and ϕ_u is the underflow solids concentration) respectively.

It is noticeable that Eq. (1) only can be solvable with proper constitutive relations. The fundamental constitutive relation for hindered settling modeling is the Kynch's assumption that the hindered settling velocity is solely determined by the local solids concentration. Based on the Kynch's assumption, three alternative methods have been established to develop the required constitutive function: the hindered settling factor approach (Buscall and White, 1987; Landman et al., 1988; Usher and Scales, 2005; Gladman et al., 2010), the Darcy's Law approach (Karl and Wells, 1999; Kinnear, 2002) and Kynch flux density approach (Bürger et al., 2000, 2005). However, the Kynch's assumption is not a nostrum, since it can only provide a complete settling behavior description of Kynchian suspensions with no compressive behavior at any concentration. Otherwise, its validity can only be proved in hindered settling region, where the concentration is sufficiently low that no weight-bearing network formed (Dixon, 1977).

When in high concentration range, where strong particle-particle interaction exists, compression settling occurs because of the compressive stress transmitted through the formed net structure (de Kretser et al., 2003), and modeling the compression settling process is significant for applications as diverse as thickening, dewatering, filtration and centrifugation. Two parallel theories have been developed to interpret the compression settling: geotechnical approach (Bürger, 2000; Bürger et al., 2001), which quantifies the sediment compressibility by using effective solids stress or the solids pressure; compression rheology approach (Buscall et al., 1987; Buscall and White, 1987), where the compressibility is characterized as the physically measurable network strength: compressive yield stress. The effective solid stress and solid pressure are usually defined as solid volumetric concentration dependent functions rather than the intrinsic material property as the compressive yield stress is. Except for the significant conceptual difference, these two approaches actually have a similar rheological basis, thus making them parallel (de Kretser et al., 2003).

The development of settling theory including the hindered and compression rheology is the first step for model formula complementation, and solving these PDEs, which means accurately solution calculation, is equivalently important for reliable model predications. When hindered settling dominates, the model governing equation can be written as Eq. (1), nonlinear hyperbolic PDEs, known as the convection-dominant model. The compression effect can be modeled by adding a nonlinear diffusion term to Eq. (1), and then the model formula becomes strongly degenerate parabolic PDEs, known as the convection-compression model (Bürger et al., 2012). Though differing in rheology basis, both convection-dominant and convection-compression models possess the similar mathematical characteristics, and solving the compression including model will not greatly increase the solution technique complexity (Bürger et al., 2012). Therefore, from a mathematical point of view, it is informative to fully understand the mathematical implication of Eq. (1) before investigating more complex models (Diehl, 2000).

Based on the mass continuity law and Kynch's assumption, the advantage of Eq. (1) is that it is capable to capture the movement of large concentration discontinuities without knowing their physical mechanisms (Kynch, 1952). However, solution discontinuities, which can be physically interpreted as the concentration gradients, are expected to occur as a function of time and height in solving Eq. (1), and greatly increases the complexity of required solution techniques. Solving Eq. (1) can be either numerical or analytical: numerical techniques including Method G (Jeppsson and Diehl, 1996), Method EO (Bürger et al., 2005), Method YRD (Li and Stenstrom, 2014a, 2014b) et al. have achieved some degree of success in shock capturing and solution calculation, but cannot always satisfy practical application standards, such as high accuracy but low computation burden; the only available approach for analytical solution construction is the method of characteristics (MOC), which avoids complicate discretization procedure but provide high accuracy solutions. Therefore, it is worthwhile further investigating the implementation strategy of MOC in 1-D continuous settling modeling.

The application of MOC to gravity settling problem can trace its history to 1950s, when Kynch (1952) analyzed the solids concentration distribution within the batch settling cylinder by using constant concentration lines, or iso-concentration lines, which is mathematically equivalent to characteristics. Thereafter, this approach was widely applied in practical SST design and operation (Fitch, 1979, 1983, 1993). In recent studies, Diehl (2007) showed that the inverse problem of estimating of the batch settling flux function from experimental data can also be well addressed by using MOC. The first MOC study in continuous settling modeling was provided by Petty (1975) to show that the limiting flux, commonly observed in lab and full scale tests, is an intrinsic nonlinear phenomenon of the governing nonlinear hyperbolic PDEs, which is lately supported by Chancelier et al. (1997) and Diehl (2008), and the propagation of solution discontinuities from bottom boundary is caused by interaction of rarefaction waves. Nevertheless, Petty's work is a MOC based continuous settling behavior analysis more than an analytical solution developing study. Hence, further investigations were motivated to complement the MOC theory in continuous settling study, including the global weak solution construction (Bustos, 1988; Bustos et al., 1990; Diehl, 1997), boundary condition determination (Bustos and Concha, 1992; Diehl, 1996, 2000), and control theory development (Buscall et al., 1982, 1990; Diehl, 2005, 2006).

The first goal of this paper is to construct solutions of the ideal SST model that includes hindered settling and hydraulic bulk transport with dynamic loading conditions on the basis of the previously developed MOC implementation strategy. The MOC solutions are compared with experimental continuous settling data to demonstrate the accuracy of MOC solutions in predicting dynamic continuous settling behaviors. Given that numerical solution techniques are often used for continuous settling models, the second part of this paper focuses on the convergence analysis of three representative numerical methods: Method SG, Method G and Method YRD by using the MOC solutions as reference solutions. Accuracy and computation cost of these three methods are also investigated to compare their efficiency for practical engineering applications. The techniques demonstrated here for solving hyperbolic PDEs are applicable in other chemical engineering problems; for example, modeling of two-phase flow in heterogeneous media (Vanduijn et al., 1995) and the investigation of multicomponent separation (adsorption, ion exchange, chromatography) when the liquid phase is plug flow (Loureiro and Rodrigues, 1991).

2. MOC theory review in ideal continuous settling model solving

To improve the understanding of the MOC theory in ideal continuous settling process and its implementation stretegy, we proived a brief reivew of the MOC theory and its implementation stretegy which is developed in previous publicitions (Diehl, 1996, 1997, 2000). For the overall SST domain, as shown in Fig. 1, the height of the clarification zone is H, and the depth of thickening zone is D. The downward direction is defined as the positive direction of the x-axis, and settling velocity and flux are positive in downward direction. The direction of feed flow (Q_f), effluent flow (Q_e), and underflow (Q_f) are also shown in Fig. 1. The Kynch's assumption (Kynch, 1952), is assumed to hold, therefore the settling velocity (v_s) as well as the Kynch batch flux function $f_{bk} = v_s\phi$ is only determined by local solids concentration ϕ. The mass conservation law model equation, Eq. (1), inside the SST domain, can be written as Eq. (2) (Diehl, 2000):

$$\begin{aligned}
&\frac{\partial\phi}{\partial t} - v_e\frac{\partial\phi}{\partial x} = 0 && x < -H\\
&\frac{\partial\phi}{\partial t} + (f'_{bk}(\phi) - v_e)\frac{\partial\phi}{\partial x} = 0 && 0 > x > -H\\
&\frac{\partial\phi}{\partial t} + (f'_{bk}(\phi) + v_u)\frac{\partial\phi}{\partial x} = 0 && D > x > 0\\
&\frac{\partial\phi}{\partial t} + v_u\frac{\partial\phi}{\partial x} = 0 && x > D
\end{aligned} \tag{2}$$

where $f'_{bk}(\phi) = d(f_{bk}(\phi))/d\phi$. As a nonlinear hyperbolic PDE, Eq. (2) possesses the property that, the initial concentration value, $\phi(x,0)$, propagates with the speed $f'_{bk}(\phi(0,x))$, along a straight line x_l with slope $x'_l = f'_{bk}(\phi(0,x))$. These straight lines with constant solutions are called *characteristics*. If the initial concentrations are not uniform, characteristics with different slopes can intersect in the positive direction of t and generate solution discontinuities, which means for a discontinuity $X = X(t)$, the solutions are ϕ^{x+} and ϕ^{x-} on the left and right side respectively, instead of being continuous.

Since the differential formula requires differentiable solutions, it cannot model the possible nondifferentiable discontinuities, thus making Eq. (2) not sufficient to completely describe the settling processes in both smooth and discontinuous regions. To provide a unique solution, the differential formula, Eq. (2), is supplemented by a jump condition (Rankine–Hugoniot relations), which is derived from the integral form, and expressed as a discontinuity $X = X(t)$, propagating at a speed of S:

$$S = z'(t) = \frac{f_{bk}(\phi^{x+}) - f_{bk}(\phi^{x-})}{\phi^{x+} - \phi^{x-}} \tag{3}$$

And Eq. (3) implies that

$$S = f'_{bk}(\xi) \tag{4}$$

where ξ is between ϕ^{x+} and ϕ^{x-}. However, given the fact that the flux function, f_{bk}, is always nonconvex, the jump condition for nonconvex scalar conservation law is not sufficient to select the unique ϕ^{x+} and ϕ^{x-} along discontinuities. A stronger condition called Oleinik entropy condition (Oleinik, 1964), is always introduced as an algebraic inequality to reject unstable discontinuities, shown as Eq. (5):

$$\frac{f_{bk}(\xi) - f_{bk}(\phi^{x-})}{\xi - \phi^{x-}} \geq S = \frac{f_{bk}(\phi^{x+}) - f_{bk}(\phi^{x-})}{\phi^{x+} - \phi^{x-}} \geq \frac{f_{bk}(\xi) - f_{bk}(\phi^{x+})}{\xi - \phi^{x+}} \tag{5}$$

for all ξ between ϕ^{x+} and ϕ^{x-}. The Oleinik entropy condition is derived from the second law of thermodynamics, and states that the flux function, f_{bk} here, lies entirely above the chord connecting ϕ^{x+} and ϕ^{x-} for $\phi^{x+} > \phi^{x-}$, or the flux function f_{bk} lies entirely below the chord connecting ϕ^{x+} and ϕ^{x-} for $\phi^{x+} < \phi^{x-}$, thus no intersection is allowed between the flux function curve and the chord.

Because of the discontinuities of flux functions at three boundaries ($x = -H$, $x = 0$, $x = D$), the solutions of the governing PDE, Eq. (2), are also discontinuous, which can be defined as following:

$$\begin{aligned}
&\phi^{-H+} = \lim_{\varepsilon\searrow 0}\phi(-H+\varepsilon, t), && \phi^{-H-} = \lim_{\varepsilon\searrow 0}\phi(-H-\varepsilon, t) && \textit{top outlet boundary}\\
&\phi^{0+} = \lim_{\varepsilon\searrow 0}\phi(0+\varepsilon, t), && \phi^{0-} = \lim_{\varepsilon\searrow 0}\phi(0-\varepsilon, t) && \textit{inlet boundary}\\
&\phi^{D+} = \lim_{\varepsilon\searrow 0}\phi(D+\varepsilon, t), && \phi^{D-} = \lim_{\varepsilon\searrow 0}\phi(D-\varepsilon, t) && \textit{bottom outlet boundary}
\end{aligned} \tag{6}$$

The mass conservation law should also hold on the three boundaries, yielding the following jump conditions:

$$\begin{aligned}
&-v_e\phi^{-H-} = v_s\phi^{-H+} - v_e\phi^{-H+} \Rightarrow g_e(\phi^{-H-}) = g(\phi^{-H+}) && \textit{top outlet boundary}\\
&v_s\phi^{0+} + v_u\phi^{0+} = v_s\phi^{0-} - v_e\phi^{0-} + s \Rightarrow f(\phi^{0+}) = g(\phi^{0-}) + s && \textit{inlet boundary}\\
&v_u\phi^{D+} = v_s\phi^{D-} + v_u\phi^{D-} \Rightarrow f(\phi^{D-}) = f_u(\phi^{D+}) && \textit{bottom outlet boundary}
\end{aligned} \tag{7}$$

Accurately determining the six boundaries solutions are especially significant, since they are not only the solutions of the governing PDEs, but also the required model outcomes, such as the effluent solids concentration (ϕ^{-H-}) and the recycle solids concentration (ϕ^{D+}). However, the jump conditions (Eqs. (3) and (7)) are not sufficient to determine the unique discontinuous solutions at three boundaries for a given initial condition. In order to select the physically acceptable boundary solutions, MOC theory at boundaries are supplemented by the *condition Γ* (Diehl, 1995, 1996), which is a generalization of Oleinik entropy condition (Eq. (5)) and motivated physically by a conservative numerical method: Godunov method (Godunov, 1959).

- top outlet boundary: to construct the physically correct ϕ^{-H-} and ϕ^{-H+}, two auxiliary functions are developed, including the non-increasing function $\breve{g}_e$ and the non-decreasing function $\hat{g}$, as shown in Eq. (8):

$$\breve{g}_e = g_e = -v_e\phi$$

$$\hat{g} = \begin{cases} \min_{\alpha\in[\phi,\phi_0]} g(\phi), & 0 \leq \phi \leq \phi_0\\ \max_{\alpha\in[\phi_0,\phi]} g(\phi), & \phi_0 \leq \phi \leq \phi_{\max}\end{cases} \tag{8}$$

where ϕ_{max} is the maximum packing concentration, an intrinsic property of the settling material. *Condition Γ* states that the effluent boundary flux γ is the value of the intersection of $\breve{g}_e$ and $\hat{g}$, and the boundary solutions ϕ^{-H-} and ϕ^{-H+} satisfy:

$$g_e(\phi^{-H-}) = \gamma = g(\phi^{-H+}) \tag{9}$$

inlet boundary: the most complex behavior of the SST occurs at the inlet, and in a fashion similar to the top outlet boundary, two auxiliary functions are introduced: the non-increasing function $\breve{g}$ and the non-decreasing function $\hat{f}$, shown as Eq. (10).

$$\begin{aligned}
&\breve{g} = \begin{cases} \max_{\alpha\in[\phi,\phi_0]} g(\phi) + s(t), & 0 \leq \phi \leq \phi_0\\ \min_{\alpha\in[\phi_0,\phi]} g(\phi) + s(t), & \phi_0 \leq \phi \leq \phi_{\max}\end{cases}\\
&\hat{f} = \begin{cases} \min_{\alpha\in[\phi,\phi_0]} f(\phi), & 0 \leq \phi \leq \phi_0\\ \max_{\alpha\in[\phi_0,\phi]} f(\phi), & \phi_0 \leq \phi \leq \phi_{\max}\end{cases}
\end{aligned} \tag{10}$$

Condition Γ states that the flux value γ at *the* feed boundary is the value of the intersection of the $\breve{g}(\phi^{0-})$ and $\hat{f}(\phi^{0+})$, and ϕ^{0-} and ϕ^{0+} satisfy:

$$f(\phi^{0+}) = \gamma = g(\phi^{0-}) + s(t) \tag{11}$$

- bottom outlet boundary: the bottom outlet boundary solutions are constructed by defining another two auxiliary functions: a non-increasing function $\breve{f}$ and a non-decreasing function $\hat{f}_u$:

$$\breve{f} = \begin{cases} \max_{\alpha \in [\phi, \phi_0]} f(\phi), & 0 \le \phi \le \phi_0 \\ \min_{\alpha \in [\phi_0, \phi]} f(\phi), & \phi_0 \le \phi \le \phi_{\max} \end{cases} \tag{12}$$
$$\hat{f}_u = f_u = v_u \phi$$

Condition Γ states that the flux value γ at *the* feed boundary is the value of the intersection of the $\breve{f}(\phi^{D-})$ and $\hat{f}_u(\phi^{D+})$, and ϕ^{D-} and ϕ^{D+} satisfy:

$$\breve{f}(\phi^{D-}) = \gamma = \hat{f}_u(\phi^{D+}) \tag{13}$$

As can be seen, the MOC theory in continuous settling includes two main parts: determining the unique correct solutions inside the SST domain by considering the jump condition and Oleinik entropy condition, and determining the unique boundary solutions by applying *condition Γ*. The most important but difficult task when using MOC is to correctly determine possible discontinuities, and the corresponding discontinuity solutions. To avoid presenting the complicated mathematics, we assume that readers are familiar with the techniques and concepts discussed above, and more information about the jump condition, Oleinik entropy condition, and *condition Γ*, can refer to (Oleinik, 1964; Diehl, 1995, 1996, 2000).

3. Continuous sedimentation experiments and model parameter estimation

It is well known that the solids handling capacity of a SST is limited, and the maximum solids flux that can be transported to the tank bottom outlet without causing changes, such as the sediment height propagation, is defined as the limiting flux (Diehl, 2005). Hence, the SST's operating conditions can be divided into three categories: (1) underloading condition if the feed flux is less than the limiting flux; (2) critical loading if the feed flux equals to the limiting flux; (3) overloading if the feed flux is larger than the limiting flux. The SST is normally underloaded, while overloading can be caused by hydraulic shock loading (wet weather) or settleability deterioration, and often leads to process failure.

Tracy (1973) conducted a lab-scale investigation of the impact of various feeding conditions on continuous settling behavior, especially the responses of the recycle concentration and sediment height. Ferric hydroxide was used as the settling material, and its settleability was characterized by the Kynch batch settling function (f_{bk}) based on the Vesilind equation (Vesilind, 1968), shown as Eq. (14):

$$f_{bk} = v_s \phi$$
$$v_s = v_0 \exp(-n\phi) \quad (\textit{Vesilind equation}) \tag{14}$$

In this study, the Vesilind parameter estimation (V_0 and n) is performed by fitting the Vesilind equation on the measured settling velocity data, and the objective function used to quantify the quality of the fit is the sum of squared errors. Table 1 shows the tank configuration and Kynch batch settling function parameters. Three transients are imposed: underloading-to-underloading, underloading-to-overloading, overloading-to-underloading by two influent forcings, and the operating condition for each transient is given in Table 2. In next section, we will show the implementation strategy of MOC to construct solutions of these three transients.

Table 1
SST configuration and Vesilind equation parameters.

SST configuration		Vesilind equation parameters	
Cross-section area [m^2]	0.0153	V_0 [m/h]	3.163
SST height [m]	2.44	n [m^3/kg]	0.936
Inlet height (m)	1.83		

4. MOC solutions construction of three transients

Each of the following three cases is designed to show how the ideal continuous settling model can be solved with MOC to show the dynamic performance. The selected cases show important and commonly observed conditions for full scale SSTs.

- Underloading–underloading transient: in this case, the change of feed flux causes a change of the recycle concentration. Hence, the MOC solution is expected to accurately predict the recycle solids concentration.
- Underloading–overloading transient: in this case, the change of feed flux causes the propagation of sediment from SST bottom, and the increase of the recycle concentration. Hence, the MOC solution is expected to accurately predict the sediment interface level and the recycle concentration to prevent process failure.
- Overloading–underloading transient: in this case, the sediment interface rises to the top due to the overloading condition and then decreases due to a reduction in feed flux. The decrease of feed flux also causes a decrease in the recycle concentration. The MOC solution is expected to accurately predict the sediment interface change including both the increase and decrease, and the recycle concentration change.

4.1. Underloading-to-underloading

For the first transient experiment, the column is initially filled with liquid, which means the initial value of the governing formula is 0. At t = 0, the tank is fed at a constant concentration (ϕ_f = 1.435 kg/m^3, s_1 = 1.22 kg/(m^{2}h)). The graphs of auxiliary functions $\hat{f}(\phi; \phi^{0+})$ and $\breve{g}(\phi; \phi^{0-}) + s$ where $\phi^{0+} = \phi^{0-} = 0$ are shown in Fig. 2 (top left). Their intersection occurs at the concentration ϕ_1^{0+} and the flux value s_1. Therefore, as the *condition Γ* states, the unique boundary condition concentrations at inlet ($x = 0$) are ϕ_1^{0+} = 0.58 kg/m^3 and ϕ_1^{0-} = 0 kg/m^3, and holds until the feed concentration changes to ϕ_f = 1.335 kg/m^3, s_2 = 0.848 kg/(m^{2}h) at t = 5 h. As shown in Fig. 2 (bottom left), Z_1 is the region where characteristics with slope $f(0)$ propagate, thus making solutions at this region equal to 0. Similarly, the solution at Z_3 is ϕ_1^{0+} = 0.58 kg/m^3 determined by the characteristics with slope $f'(\phi_1^{0+})$.

Between Z_1 and Z_3, there is an expansion wave (Z_2) consisting all concentrations between the solution of Z_1 (ϕ^{0+} = 0 kg/m^3) and the solution of Z_3 (ϕ_1^{0+} = 0.58 kg/m^3). The solution $\phi(x,t)$ within Z_2 can be uniquely solved by Eq. (15) (the monotonic decreasing of f at the left side of the inflection point ensures the invertibility of f'):

$$\phi(x, t) = (f')^{-1}(x/t) \tag{15}$$

The recycling concentration (ϕ^{D+}) remains 0, until the expansion wave reaches the bottom ($z = D$) at t_1. Then ϕ^{D+} generally increases from 0 to ϕ_1^{D+} (5.406 kg/m^3) the values predicted by the *condition Γ* as the intersection of $\breve{f}(\phi; \phi_1^{D-})$ and $\hat{f}_u$ as shown in Fig. 2 (top left). Any recycle concentration between t_1 and t_2 can be determined by Eq. (16) based on the mass conservation law:

$$v_u \phi^{D+}(D, t) = f((f')^{-1}(D/t)) \tag{16}$$

Table 2
Operation conditions for the underloading–underloading, underloading–overloading, and overloading–underloading transients from Tracy (1973).

Underloading-to-underloading			Underloading-to-overloading			Overloading-to-underloading		
Operating parameter	Underloading (0–5 h)	Underloading (5–12 h)	Operating parameter	Underloading (0–5 h)	Overloading (5–16 h)	Operating parameter	Overloading (0–10 h)	Underloading (10–30 h)
Influent flow rate (l/h)	13.02	9.72	Influent flow rate (l/h)	9.72	13.02	Influent flow rate (l/h)	15.84	15.84
Underflow rate (l/h)	3.456	3.456	Underflow rate (l/h)	2.538	2.538	Underflow rate (l/h)	3.96	3.96
Influent solids concentration (g/l)	1.435	1.335	Influent solids concentration (g/l)	1.28	1.435	Influent solids concentration (g/l)	1.4	1

At $t = 5$ h, the operation condition becomes to $\phi_f = 1.335$ kg/m^3, $s_2 = 0.848$ kg/(m^2 h), and correspondingly, the inlet boundary concentrations change to $\phi_2^{0+} = 0.33$ kg/m^3 and $\phi_2^{0-} = 0$ kg/m^3 predicted by the *condition* Γ as the intersection of $\hat{f}(\phi;\phi^{0+})$ and $\breve{g}(\phi;\phi^{0-}) + s$ ($\phi^{0+} = \phi_1^{0+}$, $\phi^{0-} = 0$), Fig. 2 (top right) shows. The change of inlet boundary concentration generates the new characteristics with slope $f'(\phi_2^{0+})$, thus making Z_4 an uniform solution region ($\phi(x,t) = \phi_2^{0+}$) as Z_1 and Z_3. Since $f'(\phi_2^{0+}) > f'(\phi_1^{0+})$, a solution discontinuity ($X_1(t)$) originates at point (5,0), and propagates toward bottom. The slope of X_1 follows the jump condition as Eq. (17):

$$X_1' = \frac{f(\phi_2^{0+}) - f(\phi_1^{0+})}{\phi_2^{0+} - \phi_1^{0+}} \tag{17}$$

At $t = t_3$, X_1 reaches the bottom ($x = D$) as shown in Fig. 2 (bottom left), and causes a sudden decrease of recycling concentration from ϕ_1^{D+} (5406 g/m^3) to ϕ_2^{D+} (3755 g/m^3). Fig. 2(bottom right) shows that the recycling concentrations change predicted by MOC solutions (the generally increase from 0 to ϕ_1^{D+} (5.406 kg/m^3) at time interval (t_1–t_2), and the decrease from ϕ_1^{D+} (5.406 g/m^3) to ϕ_2^{D+} (3.755 g/m^3) at t_3) matches the experiment data very well.

4.2. Underloading-to-overloading

The SST is filled with liquid as before in the underloading-to-underloading case, thus making the initial value as 0. The underloading condition is imposed by continuously feeding the tank with the constant ferric hydroxide flow ($\phi_f = 1.28$ kg/m^3, $s_1 = 0.81$ kg/(m^2 h)). Fig. 3(top left) shows the graphs of flux and auxiliary functions used to construct boundary concentrations. The unique inlet boundary concentrations are $\phi_1^{0+} = 0.32$ kg/m^3 and $\phi_1^{0-} = 0$ kg/m^3, determined by the intersection of $\hat{f}(\phi;\phi^{0+})$ and $\breve{g}(\phi;\phi^{0-}) + s$ ($\phi^{0+} = \phi^{0-} = 0$). Solutions are shown in Fig. 3(bottom)

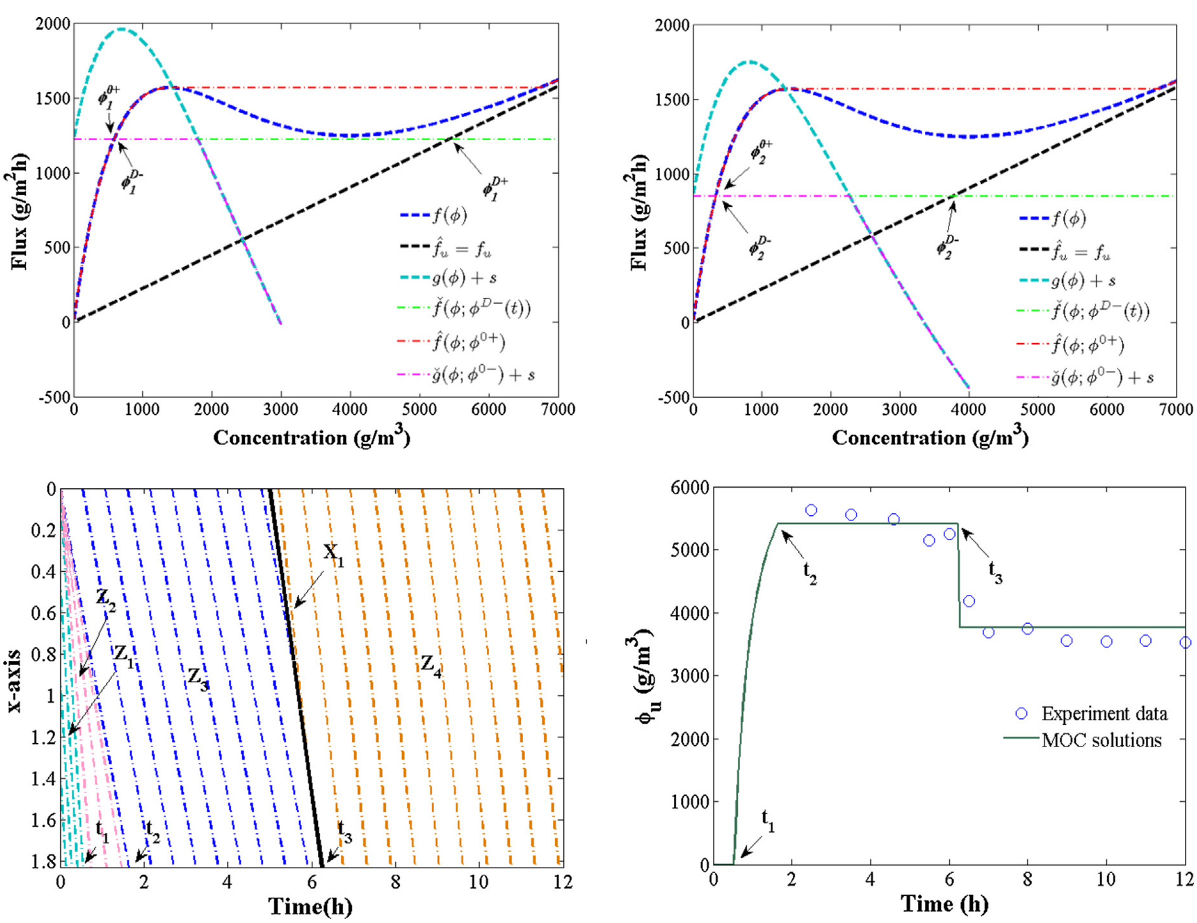

Fig. 2. Top: flux and auxiliary functions of the first underloading operation (left); flux and auxiliary functions of the second underloading operation (right). Bottom: MOC solutions of the underloading–underloading transients (left); the MOC prediction of the recycle concentration compared with the experiment observation (right).

in terms of characteristics and discontinuities. Z_1(characteristic slope = $f'\left(\phi_1^{0-}\right)$) and Z_3 (characteristic slope = $f'\left(\phi_1^{0+}\right)$) are constant solution regions with solutions as 0 kg/m^3 and 0.32 kg/m^3 respectively. The expansion wave (Z_2) between Z_1 and Z_3 includes all the concentrations between ϕ^{0+} = 0 kg/m^3 and ϕ_1^{0+} = 0.32 kg/m^3, and solutions within Z_2 can also be uniquely determined by Eq. (15). The recycle concentration (ϕ^{D+}) generally increases from 0 to ϕ_1^{D+} (4.9 kg/m^3) after the expansion wave reaches the bottom, and can be calculated by Eq. (16) as well. Therefore, the steady-state boundary concentrations are: the inlet boundary ϕ_1^{0+} = 0.32 kg/m^3 and ϕ_1^{0-} = 0 kg/m^3; the bottom boundary ϕ_1^{D+} = 4.9 kg/m^3 and ϕ_1^{D-} = 0.32 kg/m^3.

At t = 5 h, the tank is overloaded by increasing ϕ_f to 1.435 kg/m^3 (s_2 = 1.22 kg/(m^{2}h)). The intersection of $\hat{f}(\phi;\phi_1^{0+})$ and $\breve{g}(\phi;\phi_1^{0-})+s$ indicates that the inlet boundary concentrations changes to ϕ_2^{0+} = 0.62 kg/m^3 and ϕ_2^{0-} = 0 kg/m^3, see Fig. 3(top right). Since $f'\left(\phi_1^{0+}\right)$

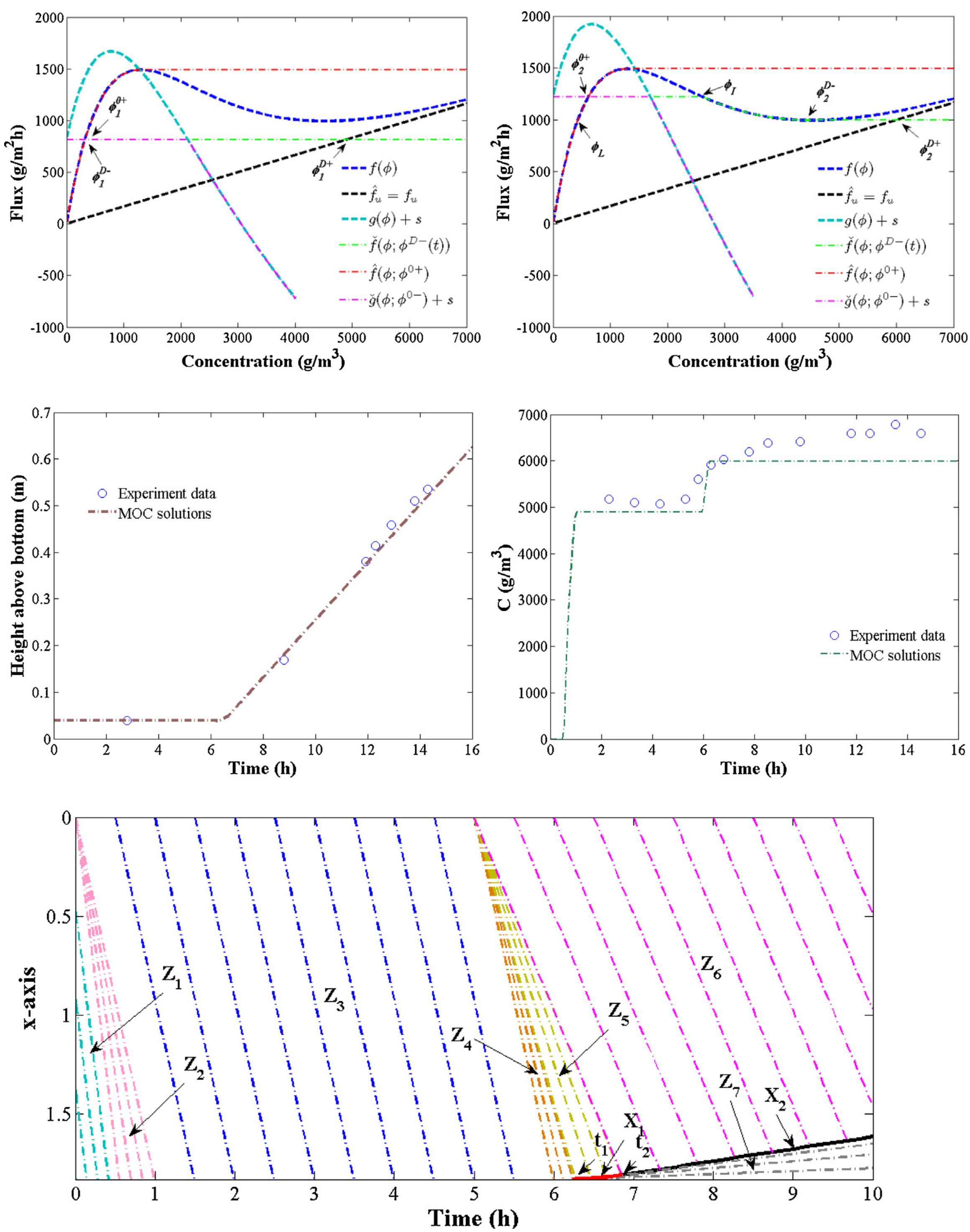

Fig. 3. Top: flux and auxiliary functions of the first underloading operation (left); flux and auxiliary functions of the second overloading operation (right). Middle: MOC prediction of sediment interface compared with the experiment observation (left); the MOC prediction of the recycle concentration compared with the experiment observation (right). Bottom: MOC solutions of the underloading–overloading transients.

$> f'\left(\phi_2^{0+}\right)$, both Z_4 and Z_5 in Fig. 3 (bottom) are expansion wave regions, at which solutions can be determined by Eq. (15), but they differ in the recycling concentration (ϕ^{D+}) change. Similar as Z_2, Z_4 causes the recycle concentration increase from ϕ_1^{D+} to ϕ_2^{D+} (6.0 kg/m^3). However, at $t = t_1$ (6.32 h), when Z_5 reaches the bottom, instead of continuously increasing the recycle concentration, a contact discontinuity ($X_1(t)$), emanates from point (D,t_1), and propagates toward the inlet ($x = 0$). Therefore, after t_1, the recycle concentration remains as ϕ_2^{D+} (6.0 kg/m^3). The solution below X_1 increases from ϕ_I to ϕ_2^{D-}, and the solution above X_1 increases from ϕ_L (the smaller solution of $f(\phi) = f(\phi_2^{D-})$) to ϕ_2^{0+} as Fig. 3(top right) shows. Complete analytical solution construction requires the determination of the formula of $X_1(t)$, the most significant but also most challenging task. Denote ϕ^{X_1-} ($\phi_L \le \phi^{X_1-} \le \phi_2^{0+}$) and ϕ^{X_1+} ($\phi_I \le \phi^{X_1-} \le \phi_2^{D-}$) as the left and right solution limits at discontinuity X_1, which satisfy Eq. (18):

$$f'(\phi^{X_1+}) = \frac{f(\phi^{X_1+}) - f(\phi^{X_1-})}{\phi^{X_1+} - \phi^{X_1-}} \tag{18}$$

Starting from (6.23, 1.83), $X_1\,(t)$ can be defined by Eq. (19):

$$\begin{aligned} \frac{X_1(t) - 0}{t - 5} &= f'(\phi^{X_1-}) \\ \frac{dX_1(t)}{dt} &= f'(\phi^{X_1+}) \end{aligned} \tag{19}$$

Since $f(\phi^{X_1+})$ can be approximated as a linear function of $f(\phi^{X_1-})$ with $R^2 = 0.998$, as Fig. 4 (left) shows, the formula of $X_1(t)$ can be determined by the following procedure:

$$\begin{aligned} \frac{dX_1(t)}{dt} &= 0.1235 \times \frac{X_1\,(t) - 0}{t - 5} - 0.1823 \\ &\Rightarrow \begin{cases} X_1(t) = \lambda \times y(t-5)^{0.1235} - 0.208 \times (t-5) \\ \qquad (1.83, 6.23) \end{cases} \Rightarrow \\ &\Rightarrow X_1\,(t) = 2.0332 \times (t-5)^{0.1235} - 0.208 \times (t-5) \end{aligned}$$

At (1.808,6.853), the intersection of X_1 and characteristics emanating at (0,5) with slope $f'(\phi_2^{0+})$, X_1 is replaced by the discontinuity X_2, which emanates tangentially from X_3. The formula of X_2 can be easily determined as $X_2(t) = X_1'(t_2) \times (t - t_2) + 1.808, \quad t_2 = 6.853$. Z_6 is a constant solution zone with $\phi(t, x) = \phi_2^{0+}$. The solution in Z_7 is determined by characteristics emanate tangentially from X_1, and for any point (x_{z_7}, t_{z_7}) in Z_7, the corresponding tangent point ($X_1(t^*)$, t^*) can be determined by Eq. (20):

$$X_1'(t^*) = \frac{x_{z_7} - X_1(t^*)}{t_{z_7} - t^*} \tag{20}$$

To accurately solve Eq. (20), numerical techniques, for example Newton's method (Traub, 1964), are needed to solve nonlinear equations. And then, the solution at (x_{z_7}, t_{z_7}) is solved based upon Eq. (21):

$$f'(\phi(x_{z_7}, t_{z_7})) = X_1'(t^*) \tag{21}$$

Fig. 3 (middle left) demonstrates the accuracy of MOC solution in sediment interface (solution discontinuities) prediction by comparing with experiment data. MOC solutions can also capture the change of recycling concentration as shown in Fig. 3 (middle right). However, the recycling concentration (6.0 kg/m^3) predicted by MOC solution in overloading condition is smaller than the experiment observation (6.6 kg/m^3). This incongruity can be attributed to the fact that the coning effect (onset of coning at the bottom of tank increases the recycling concentration but not greatly impact continuous settling behavior) and compression effect (compression effect caused by the sediment with high solids concentration produces a more concentrated recycling flow) are magnified in overloading condition, which is not considered in the ideal continuous settling model.

4.3. Overloading-to-underloading

Since settling characteristics of solids in the overloading–underloading transient cannot be adequately described by the collected batch settling data (Tracy, 1973; George and Keinath, 1978), the measured sediment interface level and recycle concentration data can be no longer used to test the MOC solution accuracy. In this case, the Vesilind parameters remain the same, and the tank operating parameters are given by Table 2.

To simplify the overloading problem analysis, the initial concentration is assumed to be the constant ϕ_0 (0.94 kg/m^3) which determined by Eq. (22) in the thickening zone, and the constant ϕ_0 (0 kg/m^3) in the clarification zone, which means the overloading will cause a sludge blanket rise in the thickening zone as time progresses, but no clarification failure in the clarification zone.

$$f(\phi_0) = \phi_f \frac{(Q_e + Q_u)}{A} = s_1 \tag{22}$$

Similarly, the inlet boundary concentrations are determined by the intersection of $\hat{f}(\phi; \phi^{0+})$ and $\breve{g}(\phi; \phi^{0-}) + s$ as $\phi_1^{0+} = 0.94$ kg/m^3 and $\phi_1^{0-} = 0$ kg/m^3, as Fig. 5(top left) shows. It is noticeable that since $\phi_0 = \phi_1^{0+}$ ($f'(\phi_0) = f'(\phi_1^{0+})$), Z_1 is a constant solution zone with the solution as ϕ_1^{0+} (0.94 kg/m^3), and the contact discontinuity X_1 emanates from bottom at $t = 0$ h, and propagates toward the inlet as a straight line. Denote the left and right solution limits of X_1 as ϕ^{X_1-} and ϕ^{X_1+}. ϕ^{X_1-} equals to ϕ_1^{0+}, and ϕ^{X_1+} can be determined by Eq. (23) (Ballou, 1970; Diehl, 2000):

$$f'(\phi^{X_1+}) = \frac{f(\phi_1^{0+}) - f(\phi^{X_1+})}{\phi_1^{0+} - \phi^{X_1+}} \tag{23}$$

Therefore, the formula of X_1 is $X_1 = f(\phi^{X_1+}) \times t + 1.83$. Below X_1, the concentration increases from ϕ^{X_1+} to ϕ_1^{D-}, and the recycling concentration remains as ϕ_1^{D+} (4.98 kg/m^3) until t_2, as shown in Fig. 5(bottom).

At $t = 10$ h, the operating condition is changed to underloading, and correspondingly, the inlet boundary concentrations change to ϕ_2^{0+} (0.45 kg/m^3) and ϕ_2^{0-} (0 kg/m^3), as Fig. 5(top right) shows. Since $f'\left(\phi_2^{0+}\right) > f'(\phi_1^{0+})$, a solution discontinuity ($X_2(t)$) originates at point (0,10), and propagates toward bottom. The formula of X_2 is $X_2(t) = X_2' \times (t - 10)$, where

$$X_2' = \frac{f(\phi_2^{0+}) - f(\phi_1^{0+})}{\phi_2^{0+} - \phi_1^{0+}} \tag{24}$$

Z_2 is a constant concentration zone with the solution of ϕ_2^{0+}. At $t = t_1$ (10.83 h), the interaction of X_1 and X_2 at (1.1, 10.83) generates the third discontinuity $X_3(t)$. Denote the left and right solution limits of X_3 as ϕ^{X_3-} and ϕ^{X_3+}. ϕ^{X_3-} equals to ϕ_2^{0+}, while ϕ^{X_3+} is in the range of ϕ_I and ϕ_1^{D-}. $X_3(t)$ is governed by Eq. (25):

$$\begin{aligned} \frac{dX_3(t)}{dt} &= \frac{f(\phi^{X_3-}) - f(\phi^{X_3+})}{\phi^{X_3-} - \phi^{X_3+}} = f'(\varepsilon) \\ \frac{X_3(t) - 1.83}{t - 0} &= f'(\phi^{X_3+}) \end{aligned} \tag{25}$$

where ε is between ϕ^{X_3-} and ϕ^{X_3+}. Fig. 4(right) shows that $f(\varepsilon)$ can be approximated as a linear function of $f(\phi^{X_3+})$ with $R^2 = 0.9889$. Hence, the formula of X_3 can be determined by the following procedure:

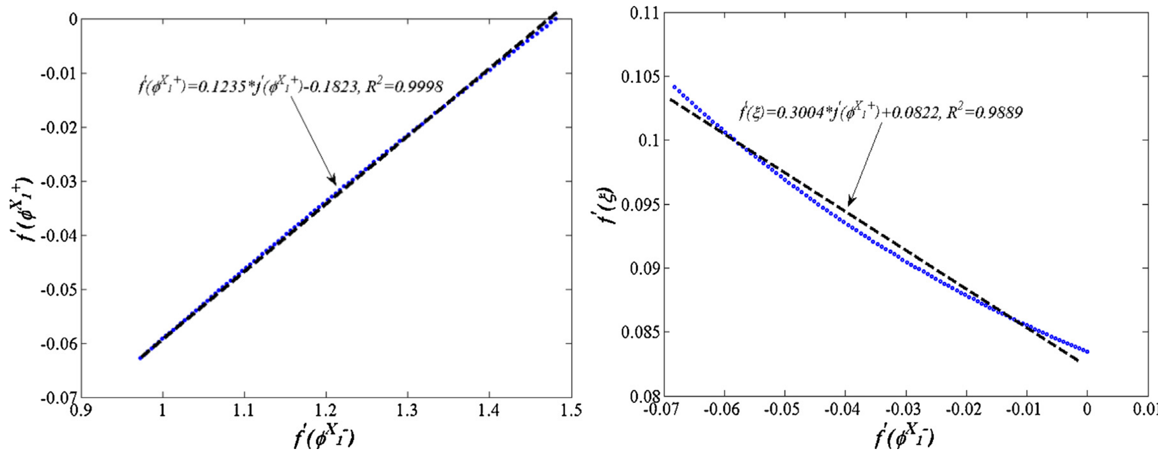

Fig. 4. approximating $f(\phi^{X_1+})$ as a linear function of $f(\phi^{X_1-})$ in underloading–overloading transient (left); approximating $f(\varepsilon)$ as a linear function of $f(\phi^{X_3+})$ in overloading–underloading transient (right).

$$\begin{aligned}\frac{dX_3(t)}{dt} &= -0.3004\times\frac{X_3(t)-1.83}{t-0}+0.0822\\ &\Rightarrow \left\{\begin{array}{l} X_3(t)=\dfrac{1.83\times t+0.0632\times t^2}{t}+\dfrac{\lambda}{t^{0.3004}}\\ (1.1,10.83)\end{array}\right. \Rightarrow X_3(t)\\ &=\frac{-2.8113\times t+1.83\times t^{1.3004}+0.0632\times t^{2.3004}}{t^{1.3004}}\end{aligned}$$

The solution in Z_3 can be determined by solving Eq. (26):

$$f'(\phi(t_{z_3},x_{z_3}))=\frac{x_{z_3}-1.83}{t_{z_3}-0} \tag{26}$$

5. Convergence analysis and efficiency comparison of numerical methods

Although MOC has been successfully implemented to develop analytical solutions, as shown previously, its application as an alternative solution technique in commercial simulators remains as a challenge for two reasons: (1) the model formula cannot always be expected to have analytical solutions, especially when it is extended to capture more physical phenomena, such as the hydrodynamic dispersion and the compression effects; (2) MOC's theoretical complexity requires considerably more effort to implement in engineering practice. Therefore, numerical solution techniques are often needed to provide accurate results.

Applied mathematical investigations have led to several alternative numerical methods, represented here by Method G based on the Godunov numerical flux (Jeppsson and Diehl, 1996; Diehl and Jeppsson, 1998), Method EO based on the Engquist–Osher numerical flux (Bürger et al., 2005), and Method YRD, a total variation diminishing (TVD) method based on flux-limit technique (Li and Stenstrom, 2014a). All these numerical methods are expected to be reliable, which means they produce approximate solutions that converge to the exact solutions as the discretization is refined (Bürger et al., 2012). However, due to the difficulty of proving convergence, only the convergence of Method EO has been proven by Bürger et al. (2005). An approach to evaluating the accuracy of the other methods is to use solutions generated by solving the model formula with Method EO at extreme high discretization level, such as 2430-layer (Bürger et al., 2012) and use this as the reference for other solutions. The successful implementation of MOC, in this study, provides another alternative approach of using analytical solutions as reference solutions.

Since the convergence of Method EO has already been proven, we did not include it in the convergence test, but added another alternative method: Method SG (simplified Godunov), which was originally proposed by Bürger et al. (2012, 2013). As the name implies, Method SG is derived from Method G, and Eq. (27) compares methods G and SG, for the thickening zone.

$$\begin{aligned} F^{G}_{i+1/2} &= \begin{cases}\min\limits_{C_i\le C\le C_{i+1}}(v_s\phi+v_u\phi) & \text{if}\quad \phi_i\le\phi_{i+1}\\ \max\limits_{C_{i+1}\le C\le C_i}(v_s\phi+v_u\phi) & \text{if}\quad \phi_i>\phi_{i+1}\end{cases}\\ F^{SG}_{i+1/2} &= \begin{cases}\min\limits_{C_i\le C\le C_{i+1}}(v_s\phi)+v_u\phi & \text{if}\quad \phi_i\le\phi_{i+1}\\ \max\limits_{C_{i+1}\le C\le C_i}(v_s\phi)+v_u\phi & \text{if}\quad \phi_i>\phi_{i+1}\end{cases}\end{aligned} \tag{27}$$

where i is layer index; F^G is the Godunov numerical flux; F^{SG} is the simplified Godunov numerical flux. As can be seen, both of Method G and Method SG are based on Godunov numerical flux, but differ in the numerical flux application: Method G applies the Godunov flux to the total flux, while Method SG applies the Godunov flux only to the nonlinear settling flux ($v_s\phi$); the linear bulk flux ($v_u\phi$) is unchanged. This adjustment leads to a simplification in determining the local extrema: Method G, Method EO, Method YRD require keeping track of two local extremum of the total flux function, which may vary with the change of underflow rate, while Method SG only requires the determination of only one local extrema that does not vary with underflow rate, thus making Method SG easier to implement with the algorithm given by Bürger et al. (2013).

To evaluate convergence, various model outputs have been obtained using a reliable solution technique, which are then used as a reference solution. For example, Bürger et al. (2012) used the concentration profile from Method EO to validate Method G. In this study, the sludge blanket level is selected for comparison for two reasons: (1) sludge blanket level is one of the most significant model outputs for system robustness evaluation; (2) the shock path (sludge blanket level) function developed by MOC can be directly applied to test the shock capturing accuracy, generally the most challenging task in a numerical solution. The spatial and time steps are same for all three methods, and the discretization level starts at 40-layer as Jeppsson and Diehl (1996) recommended. Solutions of the underloading–overloading scenario (scenario 1) and overloading–underloading scenario (scenario 2) as shown in Table 2 are solved with Methods SG, G and YRD to demonstrate and compare their convergences.

The sludge blanket levels for both loading conditions at discretization levels of 40, 100 and 200-layer by Methods SG, G and YRD are shown in Fig. 6, and compared with the MOC solution. As

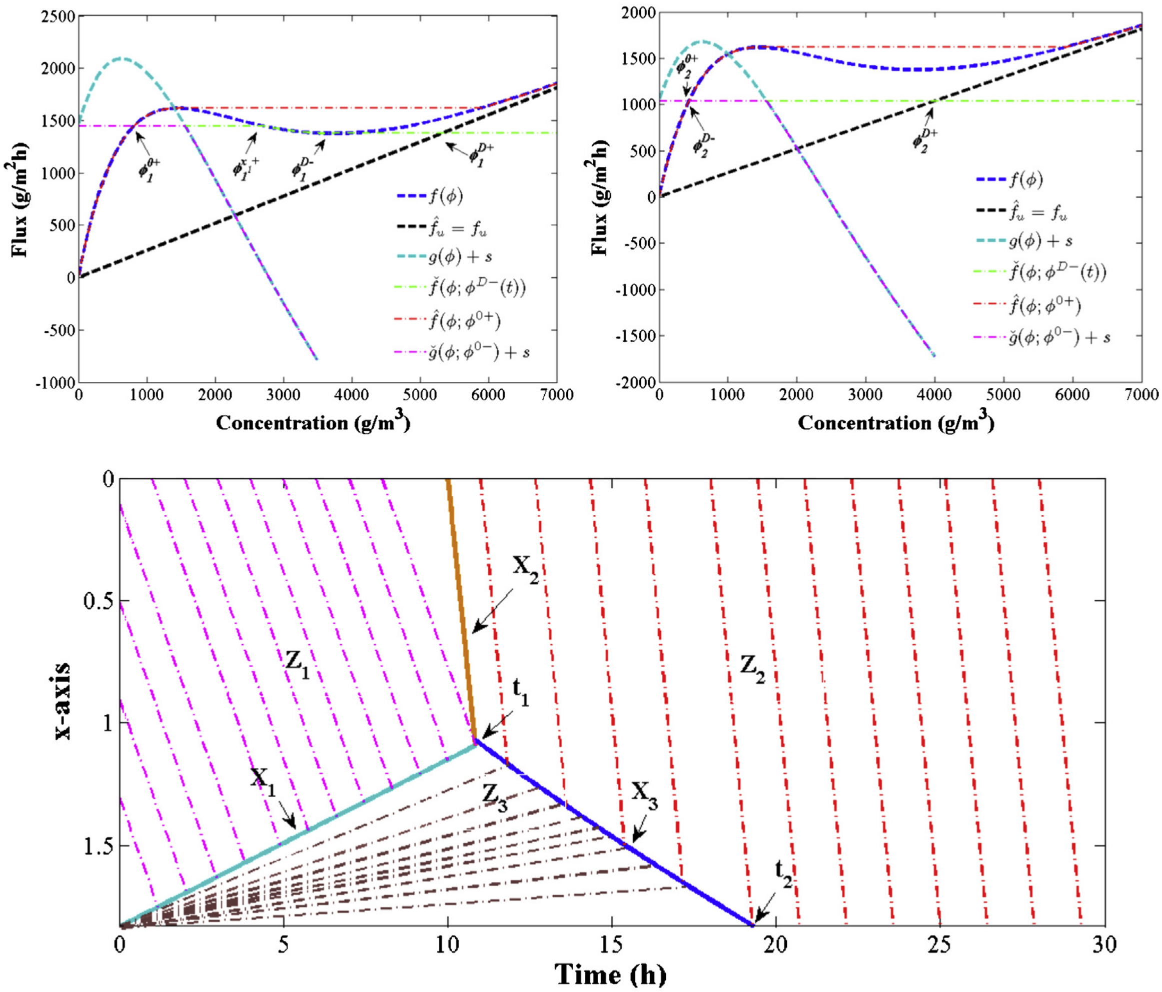

Fig. 5. Top: flux and auxiliary functions of the first overloading operation (left); flux and auxiliary functions of the second underloading operation (right). Bottom: MOC solutions of the overloading–underloading transients.

can be seen, all these three methods are able to track the change of the sludge blanket level regardless of the discretization level. For each method, the approximate solution for 40-layer deviates most from the reference, but as the discretization increases (increasing number of layers), the approximate solutions converge to the reference solutions, as demonstrated. The convergence rate with increasing discretization is rapid at first, but greatly decreases as the number of layers approaches 500, which is most evident in the Method SG simulation results.

Even though Fig. 6 qualitatively shows that all three methods are able to converge to reference solutions, at least in these two scenarios, it does not mean they are equally efficient in practical engineering applications. An efficient numerical method is defined as high in approximation accuracy and low in computation cost. To further quantify the efficiency of these three alternatives, computation cost is characterized by the required CPU time, and accuracy is evaluated using the error measurement defined in Eq. (28).

$$e_h = \frac{\sum_{j=1}^{m}\left(\left|h_j^N(t) - h_j^R(t)\right| / h_j^R(t)\right)}{m} \tag{28}$$

where e_h is the averaged relative error in sludge blanket level; j is the time index; m is the overall time step used; h denotes the sludge blanket level; N is the discretization level, and R denotes the reference solution. The amount of required memory can also be important in defining efficiency, but it is not important in this case since the needed memory can be provided by a typical desk top computer.

Fig. 7 (left) shows the e_h change with increasing discretization, and quantitatively confirms the conclusion made previously that for these three methods, increasing discretization can effectively improve the quality of numerical solutions, but yields diminishing returns when using a large number of layers. Method YRD shows the most relative improvement with increased number of layers, but its absolute accuracy is much greater that Method G and SG for any fixed N. For example, Method YRD using 40-layer has approximately the same accuracy as Method G using 200-layer and much more accurate than Method SG using 200-layer. This difference in accuracy can be attributed to the fact that Method YRD possesses second-order accuracy in both smooth and discontinuous regions, while Method G is first-order accurate. At the same discretization level, Method SG can be no more accurate than Method G because the simplification in numerical flux that facilitates implementation results in increased numerical errors (Bürger et al., 2012; Li and Stenstrom, 2014a).

Nevertheless, Method YRD's error reduction is at the cost of more computation, which is quantitatively indicated by the increase of CPU time shown in Fig. 7 (right); less CPU time means fewer computations and faster simulations. Method SG produces approximations faster than the other two methods for any given N. If CPU time is further approximated as a linear function of the discretization, the rate of computation increase for Method YRD, Method G and Method SG is 0.31 s/layer, 0.22 s/layer, 0.07 s/layer,

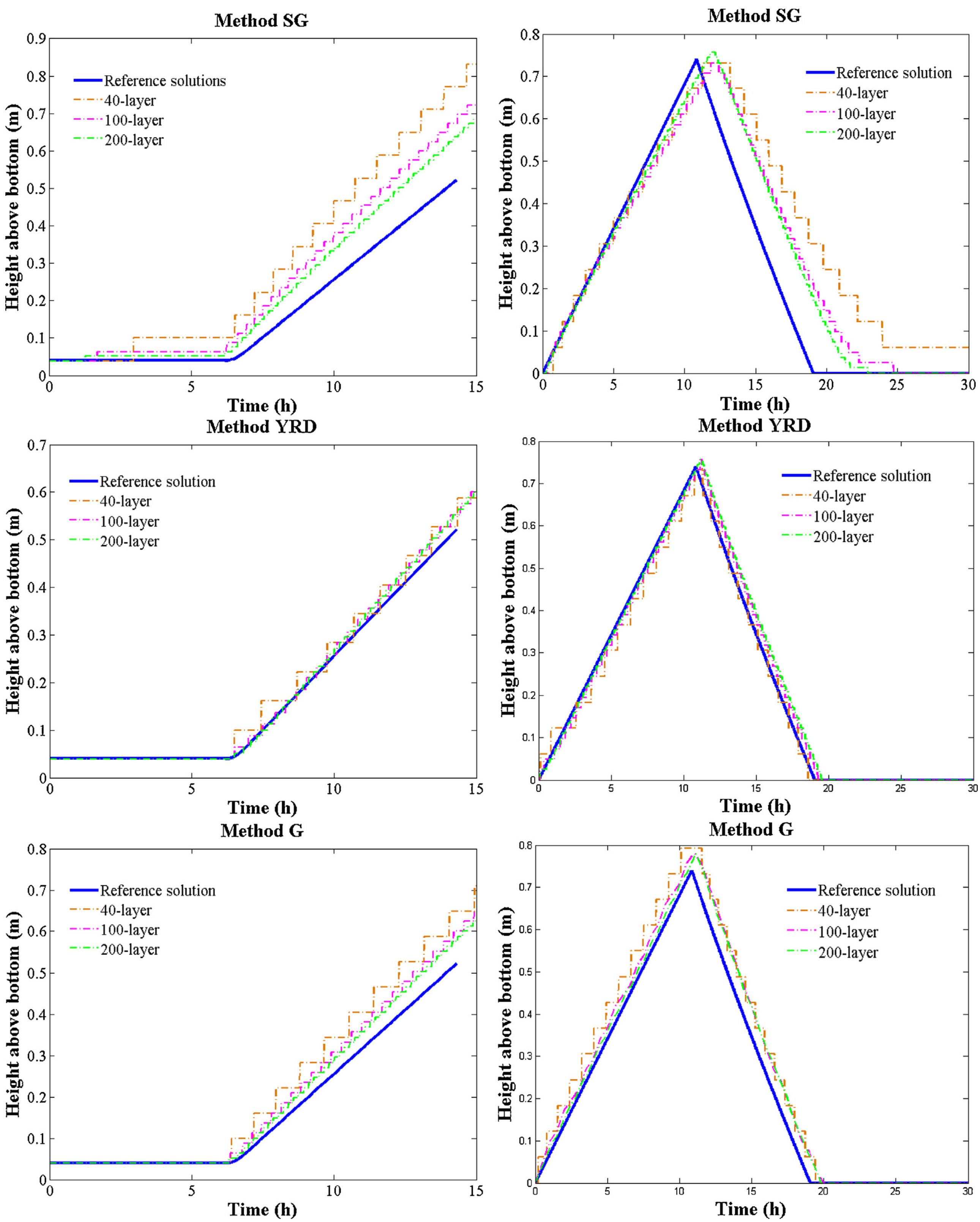

Fig. 6. Comparison of solution convergences for Methods SG, YRD and G (top to bottom, respectively) for the two cases of under loading-to-overloading and overloading-to-under loading (left to right, respectively) at $N = 40,100,200$.

respectively, which implies that Method YRD requires much more computations than the other two. For example the computation cost of Method YRD at 100-layer equals to it of Method G at 197-layer and Method SG at 475-layer. It seems that we might be able to continuously refine the discretization of Method G and Method SG to make them as accurate as Method YRD in numerical calculation but with the same or even less computation cost. Nevertheless, this strategy is questionable for two reasons: (1) continuously refining discretization requires smaller time steps to guarantee calculation stability, which may invalidate the observed linear relations and

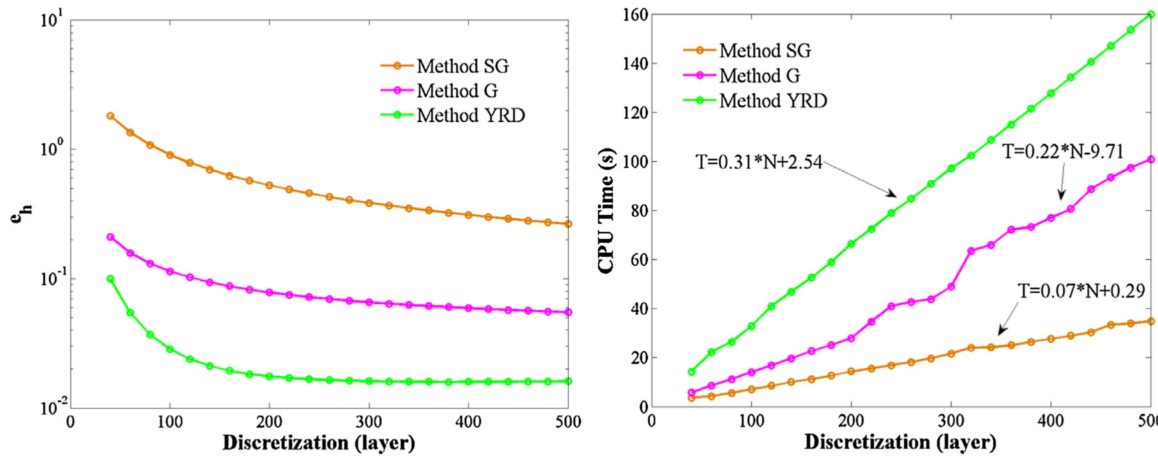

Fig. 7. Errors of the underloading–overloading transient simulation at various layer numbers (left); CPU times of the underloading–overloading transient simulation at various layer numbers (right).

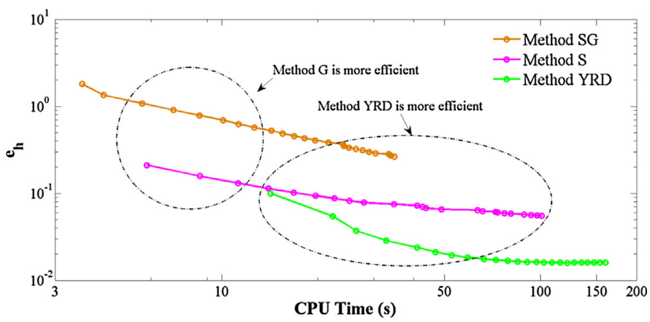

Fig. 8. Efficiency lines (error *vs.* CPU time) of Methods SG, G and YRD for different layer numbers.

make the real computation cost much more than the predicated one; (2) as shown in Fig. 6 (left), the rate of error decrease with increasing discretization decreases. Methods SG and G will require greater levels of discretization to obtain a specified accuracy. The choice of method will depend upon the required accuracy and the availability of computing resources.

Fig. 8 shows the efficiency line of each method based Fig. 6. If the computation cost is the priority (CPU time < *20*s), Method G and Method SG can be the only two alternatives, and Method G is more efficient than Method SG as its efficiency line lies below that of Method SG. However, if the accuracy is the priority ($e_h < 10^{-1}$), Method YRD is the most efficient one regard less of its high implementation complexity. The implementation complexity (complexity of the computer code) of the three methods cannot be included in Fig. 8, since it is difficult to quantify. Based on our knowledge, more accurate calculation of the numerical flux usually complicates implementation; the simplification of the Godunov numerical flux calculation makes the implementation of Method SG much easier than it of Method G, while the flux limited technique used in Method YRD to ensure a second-order accuracy can greatly increase the implementation complexity.

6. Conclusion

Accurately solving the ideal continuous settling model is challenging because of solution discontinuities. As the only available method for analytical solution development of ideal continuous settling model, the method of characteristics has been successfully implemented to investigate the dynamics of SST for three typical solids loading transients: underloading–underloading, underloading–overloading and overloading–underloading. The comparison of experiment continuous settling data and MOC solutions demonstrates that the ideal continuous settling model solved by MOC can accurately predict the recycle concentration and sediment interface change at various operation conditions. However, because of the complexity of implementing MOC, further studies are required to develop more efficient implementation strategies.

To avoid the complexity of MOC, alternative solution techniques are available but have not been extensively verified as to convergence and efficiency. By using the MOC solution as reference, the convergence analysis of Methods SG, G, and YRD shows that all are reliable, since they are able to provide arbitrary close approximations to the reference solutions as discretization is refined. An efficiency comparison based upon three completing principles: easy implementation, high accuracy and low computation cost is provided. For a given discretization level, Method YRD is most efficient in reducing error, and provides the most accurate approximations. However, this advantage of high accuracy of Method YRD is at the cost of larger computation time and coding complexity when compared with Methods SG and G. The simplified numerical flux calculation technique used in Method SG increases error, but greatly reduces the coding complexity and computation cost. Method G performs well in both accuracy and computation cost comparisons. Therefore, the selection of the most desirable numerical solution technique depends on the ease of implementation, accuracy and computation cost.

Acknowledgments

The present study was supported in part by the National Science Foundation (NSF), Award 1134355. Ben Li. received a fellowship from the University of California, Los Angeles (UCLA).

References

Ballou DP. Solutions to nonlinear hyperbolic cauchy problems without convexity conditions. Trans Am Math Soc 1970;152:441–60.

Bürger R. Phenomenological foundation and mathematical theory of sedimentation–consolidation processes. Chem Eng J 2000;80:177–88.

Bürger R, Concha F, Karlsen KH. Phenomenological model of filtration processes: 1. Cake formation and expression. Chem Eng Sci 2001;56:4537–53.

Bürger R, Concha F, Tiller FM. Applications of the phenomenological theory to several published experimental cases of sedimentation processes. Chem Eng J 2000;80:105–17.

Bürger R, Diehl S, Faras S, Nopens I. On reliable and unreliable numerical methods for the simulation of secondary settling tanks in wastewater treatment. Comput Chem Eng 2012;41:93–105.

Bürger R, Diehl S, Faras S, Nopens I, Torfs E. A consistent modelling methodology for secondary settling tanks: a reliable numerical method. Water Sci Technol 2013;68:192–208.

Bürger R, Diehl S, Nopens I. A consistent modelling methodology for secondary settling tanks in wastewater treatment. Water Res 2011;45:2247–60.

Bürger R, Karlsen KH, Towers JD. A model of continuous sedimentation of flocculated suspensions in clarifier-thickener units. SIAM J Appl Math 2005;65:882–940.

Buscall R, Goodwin JW, Ottewill RH, Tadros TF. The settling of particles through newtonian and non-newtonian media. J Colloid Interface Sci 1982;85:78–86.

Buscall R, Mcgowan IJ, Mills PDA, Stewart RF, Sutton D, White LR, Yates GE. The rheology of strongly-flocculated suspensions. J Non-Newton Fluid Mech 1987;24:183–202.

Buscall R, White LR. The consolidation of concentrated suspensions.1. The theory of sedimentation. J Chem Soc-Faraday Trans I 1987;83:873–91.

Bustos MC. On the construction of global weak solutions in the Kynch theory of sedimentation. Math Methods Appl Sci 1988;10:245–64.

Bustos MC, Concha F. Boundary-conditions for the continuous sedimentation of ideal suspensions. AIChE J 1992;38:1135–8.

Bustos MC, Paiva F, Wendland W. Control of continuous sedimentation of ideal suspensions as an initial and boundary-value problem. Math Methods Appl Sci 1990;12:533–48.

Chancelier JP, DeLara MC, Joannis C, Pacard F. New insights in dynamic modeling of a secondary settler—I. Flux theory and steady-states analysis. Water Res 1997;31:1847–56.

de Kretser RG, Scales PJ, Bagley DM. Compressive rheology: an overview. In: Binding DM, Walters K, editors. Rheology Reviews. Aberystwyth: British Society of Rheology; 2003. p. 125–66.

Diehl S. On scalar conservation-laws with point-source and discontinuous flux function. SIAM J Math Anal 1995;26:1425–51.

Diehl S. A conservation law with point source and discontinuous flux function modelling continuous sedimentation. SIAM J Appl Math 1996;56:388–419.

Diehl S. Dynamic and steady-state behavior of continuous sedimentation. SIAM J Appl Math 1997;57:991–1018.

Diehl S. On boundary conditions and solutions for ideal clarifier-thickener units. Chem Eng J 2000;80:119–33.

Diehl S. Operating charts for continuous sedimentation II: step responses. J Eng Math 2005;53:139–85.

Diehl S. Operating charts for continuous sedimentation III: control of step inputs. J Eng Math 2006;54:225–59.

Diehl S. Estimation of the batch-settling flux function for an ideal suspension from only two experiments. Chem Eng Sci 2007;62:4589–601.

Diehl S. The solids-flux theory – confirmation and extension by using partial differential equations. Water Res 2008;42:4976–88.

Diehl S, Jeppsson U. A model of the settler coupled to the biological reactor. Water Res 1998;32:331–42.

Dixon DC. Momentum-balance aspects of free-settling theory. 1. Batch Thickening. Sep Sci 1977;12:171–91.

Fitch B. Sedimentation of flocculent suspensions – state of the art. AIChE J 1979;25:913–30.

Fitch B. Kynch theory and compression zones. AIChE J 1983;29:940–7.

Fitch B. Thickening theories – an analysis. AIChE J 1993;39:27–36.

George DB, Keinath TM. Dynamics of continuous thickening. J Water Pollut Control Fed 1978;50:2560–72.

Gladman BR, Rudman M, Scales PJ. Experimental validation of a 1-D continuous thickening model using a pilot column. Chem Eng Sci 2010;65:3937–46.

Godunov SK. A finite difference method for the numerical computations of discontinuous solutions of the equations of fluid dynamics. Mat Sb 1959;47:271–306 [in Russian].

Jeppsson U, Diehl S. An evaluation of a dynamic model of the secondary clarifier. Water Sci Technol 1996;34:19–26.

Karl JR, Wells SA. Numerical model of sedimentation/thickening with inertial effects. J Environ Eng – ASCE 1999;125:792–806.

Kinnear DJ. Biological solids sedimentation: a model incorporating fundamental settling parameters. Department of Civil and Environmental Engineering, University of Utah; 2002.

Kynch GJ. A theory of sedimentation. Trans Faraday Soc 1952;48:166–76.

Landman KA, White LR, Buscall R. The continuous-flow gravity thickener – steady-state behavior. AIChE J 1988;34:239–52.

Li B, Stenstrom MK. Dynamic one-dimensional modeling of secondary settling tanks and design impacts of sizing decisions. Water Res 2014a;50:160–70.

Li B, Stenstrom MK. Dynamic one-dimensional modeling of secondary settling tanks and system robustness evaluation. Water Sci Technol 2014b;69:2339–49.

Li B, Stenstrom MK. Research advances and challenges in one-dimensional modeling of secondary settling tanks – a critical review. Water Res 2014c;65:40–63.

Loureiro JM, Rodrigues AE. Solution methods for hyperbolic systems of partial-differential equations in chemical-engineering. Chem Eng Sci 1991;46:3259–67.

Northcott KA, Snape I, Scales PJ, Stevens GW. Dewatering behaviour of water treatment sludges associated with contaminated site remediation in Antarctica. Chem Eng Sci 2005;60:6835–43.

Oleinik AO. Uniqueness and stability of the generalized solution of the Cauchy problem for a quasi-linear equation. Am Math Soc Trans Ser 1964;2:285–90.

Petty CA. Continuous sedimentation of a suspension with a nonconvex flux law. Chem Eng Sci 1975;30:1451–8.

Shannon PT, Stroupe E, Tory EM. Batch and continuous thickening – basic theory – solids flux for rigid spheres. Ind Eng Chem Fundam 1963;2:203.

Tracy KD. Mathematical modeling of unsteady-state thickening of compressible slurries. Clemson, South Carolina: Clemson University; 1973.

Traub JF. Iterative methods for solution of equations. Englewood Cliffs, NJ: Prentice-Hall; 1964.

Usher SP, Scales PJ. Steady state thickener modelling from the compressive yield stress and hindered settling function. Chem Eng J 2005;111:253–61.

Vanduijn CJ, Molenaar J, Deneef MJ. The effect of capillary forces on immiscible 2-phase flow in heterogeneous porous-media. Transp Porous Media 1995;21:71–93.

Vesilind PA. Discussion of "Evaluation of Activated Sludge Thickening Theories" By R.I. Dick and B.B Ewing. J San Eng Div ASCE 1968;94:185–91.